Analytica Chimica Acta 819 (2014) 94–101

Contents lists available at ScienceDirect

Analytica Chimica Acta

journal homepage: www.elsevier.com/locate/aca

# Nonenzymatic amperometric sensor for ascorbic acid based on hollow gold/ruthenium nanoshells

Ara Jo[a,1], Minkyung Kang[a,1], Areum Cha[a], Hye Su Jang[a], Jun Ho Shim[b], Nam-Suk Lee[c], Myung Hwa Kim[a], Youngmi Lee[a,*], Chongmok Lee[a,**]

[a] Department of Chemistry & Nano Science, Ewha Womans University, Seoul 120-750, Republic of Korea
[b] Department of Chemistry, Daegu University, Gyeongsan 712-714, Republic of Korea
[c] National Center for Nanomaterials Technology (NCNT), Pohang University of Science and Technology (POSTECH), Pohang 790-784, Republic of Korea

## HIGHLIGHTS

- We synthesized hollow gold/ruthenium (hAu–Ru) nanoshells for ascorbic acid sensing.
- The hAu–Ru nanoshells showed sensitivity of 426 μA mM$^{-1}$ cm$^{-2}$ for ascorbic acid.
- Good selectivity against glucose, uric acid, dopamine, 4-acetamidophenol, and NADH.
- The linear dynamic range appeared from zero to 2.0 mM ($R$ = 0.9995).
- Response time (1.6 s) and low detection limit (2.2 μM) were obtained at pH 7.40.

## GRAPHICAL ABSTRACT

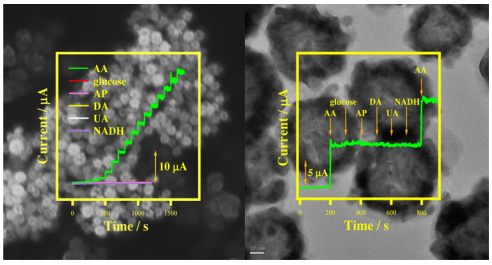


## ARTICLE INFO

*Article history:*
Received 1 November 2013
Received in revised form 21 January 2014
Accepted 12 February 2014
Available online 15 February 2014

*Keywords:*
Hollow gold ruthenium
Nonenzymatic ascorbic acid sensor
Electrocatalyst
Amperometric sensor
Biosensor

## ABSTRACT

We report a new nonenzymatic amperometric detection of ascorbic acid (AA) using a glassy carbon (GC) disk electrode modified with hollow gold/ruthenium (hAu–Ru) nanoshells, which exhibited decent sensing characteristics. The hAu–Ru nanoshells were prepared by the incorporation of Ru on hollow gold (hAu) nanoshells from Co nanoparticle templates, which enabled AA selectivity against glucose without aid of enzyme or membrane. The structure and electrocatalytic activities of the hAu–Ru catalysts were characterized by spectroscopic and electrochemical techniques. The hAu–Ru loaded on GC electrode (hAu–Ru/GC) showed sensitivity of 426 μA mM$^{-1}$ cm$^{-2}$ (normalized to the GC disk area) for the linear dynamic range of <5 μM to 2 mM AA at physiological pH. The response time and detection limit were 1.6 s and 2.2 μM, respectively. Furthermore, the hAu–Ru/GC electrode displayed remarkable selectivity for ascorbic acid over all potential biological interferents, including glucose, uric acid (UA), dopamine (DA), 4-acetamidophenol (AP), and nicotinamide adenine dinucleotide (NADH), which could be especially good for biological sensing.



## 1. Introduction

Ascorbic acid (AA, generally known as Vitamin C) and its salts are commonly used for food additives. AA, widely known as antioxidant, also plays a key role in metabolism of cholesterol. In recent

* Corresponding author.
** Corresponding author. Tel.: +82 232772344; fax: +82 232772384.
*E-mail addresses:* youngmilee@ewha.ac.kr (Y. Lee), cmlee@ewha.ac.kr (C. Lee).
[1] Authors are equally contributed to this work.

http://dx.doi.org/10.1016/j.aca.2014.02.017
0003-2670/

researches, a variety of important role of AA has been revealed in various fields such as toxicology, genetics, oncology, nutritional science, and even material science [1] as a mild reducing agent. Toxicity of reactive oxygen species [2] and synthetic pyrethroid pesticide [3] can be protected by AA reducing toxic substances. Thus, measuring AA is of great importance from food industry to medical reason. In fact, a tremendous number of studies have been reported for quantification of AA. For example, colorimetry, titrimetry, fluorometry, high performance liquid chromatography, chemiluminescence, flow injection method, and electrochemical measurement were reported [4].

While AA is important in biological process, it is also known as one of the notorious biological interfering species in detection of other biomolecules, e.g., glucose and neurotransmitters [5]. Despite of various determination methods of AA, the electrochemical methods, including amperometric [6,7], voltammetric [8,9], and potentiometric [10] methods, are considered as one of the convenient methods due to simplicity and rapidity without sample preparation procedures. Most of reported electrochemical works use either enzyme (ascorbate oxidase), mediator or conducting polymer [5] to overcome the irreversible nature of AA oxidation and enhance the selectivity and sensitivity for determination of AA.

Recently, nanostructured catalysts have been applied to nonenzymatic electrochemical biomolecule sensors since the pioneer works of glucose detection with nanoporous platinum [11–13]. For the nonenzymatic electrochemical detection of AA, uric acid (UA), and/or dopamine (DA), palladium materials were often applied via incorporation with carbon nanotube, carbon nanofiber, polymer and graphene [5,8,14–17]. 3-D nanoporous gold film was also used for electrochemical determination of DA and AA [18].

Gold nanoparticles (Au NPs) have been well known as nonenzymetic glucose oxidation catalysts [19]. However, there were some reports for AA sensing based on Au NPs [20–22], where interference by glucose were not explicitly shown up to the physiological level. Glucose is also interfering species in AA sensing, and vice versa. Meanwhile, the oxidation current of glucose decreased by plating Ru layer [23] and potential of glucose was shifted depending on the amount of incorporating Ru [30] in Au-based glucose sensing. Thus, Ru modification on the surface of Au nanoshells is one of the plausible ways to overcome glucose interference in AA sensing.

In this study, we report a new nonenzymatic amperometric AA sensor modified with the hollow gold/ruthenium (hAu–Ru) bimetallic nanoshells, which shows high selectivity for AA over possible biological interferents, including UA, DA, 4-acetamidophenol (AP), and nicotinamide adenine dinucleotide (NADH) as well as glucose, at the physiological pH. This is rare case for the gold based catalyst without aid of enzyme or membrane.

## 2. Experimental

### 2.1. Reagents

The materials and reagents used in this work are as follows: $CoCl_2{\cdot}6H_2O$, trisodium citrate ($Na_3C_6H_5O_7$), $RuCl_3{\cdot}xH_2O$, D-(+)-glucose, L-ascorbic acid (AA), 4-acetamidophenol (AP), dopamine hydrochloride (DA), uric acid (UA) and β-nicotinamide adenine dinucleotide reduced disodium salt hydrate (NADH) were purchased from Sigma–Aldrich (St. Louis, MO); $NaBH_4$ and $HAuCl_4{\cdot}xH_2O$ were purchased from Fluka (Buchs, Switzerland) and Alfa Aesar (Haverhill, MA), respectively. All other conventional chemicals used were of analytical grade. All aqueous solutions were prepared using deionized water (resistivity $\geq$18 MΩ cm$^{-1}$).

### 2.2. Synthesis of hAu–Ru nanaoshells

Before synthesizing hAu–Ru nanoshells, the hAu nanoshells were synthesized at room temperature using a slightly modified method reported in the literature [24,25]. In a typical synthesis of hAu nanoshells, 135 mL of deionized water was placed in a 250 mL beaker and situated to a nitrogen atmosphere by inserting a syringe needle over 30 min with vigorous stirring. Then, 2.5 mL of $NaBH_4$ (0.24 M) and 2.5 mL of trisodium citrate (0.12 M) were injected into water sequentially. After waiting for 5 min, 5.0 mL of $CoCl_2$ (75 mM aqueous solution) was added drop by drop while stirring and then left to stand with stirring for a while (ca. 15 min). The reaction mixture became dark brown in color at this stage due to formation of Co nanoparticles. Then 5 mL of $HAuCl_4$ aqueous solution (30 mM) was added drop-wise to obtain hAu nanoshells, where the color changed to dark blue. The hAu nanoshells were collected after 15 min by washing-centrifugation at least five times. To prepare hAu–Ru nanoshells, 5 mL of $RuCl_3$ aqueous solution (30 mM) was added drop by drop to the aforementioned product solution after 5 min (containing hAu nanoshells) and left to stand for 15 min while stirring, where the color of the solution was changed back to dark brown due to excess $RuCl_3$. The obtained samples were washed at least five times with water and collected by centrifugation for morphology and structure analysis.

### 2.3. Characterizations

For high-resolution transmission electron microscopy (HR-TEM), energy dispersive X-ray spectroscopy (EDS) and field emission scanning electron microscope (FE-SEM) sample preparation, one drop of an aqueous suspension of the nanostructures was placed on a carbon-coated copper grid (Ted Pella, Redding, CA), and allowed to dry. TEM was performed using a JEOL JEM-2100F (Cs-corrected STEM/TEM) microscope at an accelerating voltage of 200 kV. The hAu and hAu–Ru nanoshells were also characterized by scanning electron microscopy (SEM). Raman scattering measurements were directly carried out with hAu–Ru nanoshells on a transferred to a Pyrex glass slide. The backscattering configuration was employed to record the Raman spectrum using a confocal microscope with a 100× (0.9 NA) objective in focused the laser beam (~1 μm) with 632.8 nm He–Ne laser light. We kept with lower laser power to prevent from the decomposition of the sample by localized laser heating. Optimal results were obtained with 20 mW laser power and 300 s integration times. The surface properties were characterized using X-ray photoelectron spectroscopy (XPS, Theta Probe AR-XPS System, Thermo Fisher Scientific) at Busan Center, KBSI. Crystal structures were studied by X-ray diffraction (XRD; Siemens D500, with a Cu Kα radiation).

### 2.4. Electrochemical measurements

To increase the signal-to-noise ratio (S/N) all the electrochemical experiments were carried out in a Faraday cage under the nitrogen atmosphere using a CHI 705 workstation (CH Instruments, TX, USA) and an RDE-1 (BAS (Bioanalytical Systems Inc., IN, USA)). For measurements, a Pt coil and saturated calomel electrode (SCE) were used as a counter and reference electrode, respectively, with a conventional three-electrode cell. A glassy carbon (GC) electrode (3 mm in diameter, BAS) was used as the substrate electrode to modify the surface with hAu or hAu–Ru nanoshells, which served as a working electrode. Prior to modification of the electrode surface, a GC electrode was wet-polished on a microcloth pad (Buehler) using 0.3 μm alumina slurries. The electrode was cleaned with deionized

water and sonicated in $H_2O$ and ethanol for a while to remove the residual alumina from the electrode surface.

The prepared 2 mg catalyst (hAu or hAu–Ru nanoshells) was suspended in 1 mL distilled water. This mixture (10 μL) was loaded onto the GC electrode and dried under ambient conditions, which were repeated one more time. Linear sweep voltammetry (LSV) experiments for the nanoshell modified electrodes, namely hAu/GC and hAu–Ru/GC, respectively, were conducted by rotating electrodes in the potential range from −0.3 to 0.4 V (vs. SCE) with a scan rate ($\upsilon$) of 5 mV $s^{-1}$. Amperometric current response for AA and interferents was measured by monitoring current at 0.05 V with continuous stirring. All the electrochemical experiments were performed at physiological pH (7.4) in a 0.1 M phosphate buffer solution (PBS).

## 3. Results and discussion

### 3.1. Synthesis and characterization of hAu and hAu–Ru nanoshells

Since hollow metal nanoshells can be generally synthesized with Co nanoparticles as sacrificial templates [24], the formation of Co nanoparticles is critical step to control the size of hollow metal nanoshells. The formation of Co nanoparticles in the mixture of $CoCl_2$ and reducing agents can be conceived easily by the change of color from transparent to dark brown. The standard reduction potential of $Co^{2+}/Co$ redox couple (−0.28 V vs. SHE) is much lower than that of $[AuCl_4]^-/Au$ redox couple (0.99 V vs. SHE), which enables the spontaneous deposition of gold atoms to the vicinity of the outer surface of Co nanoparticles leaving interior cavity via galvanic replacement reaction (GRR), $2[AuCl_4]^-(aq) + 3Co(s) \longrightarrow 2Au(s) + 3Co^{2+}(aq) + 8Cl^-(aq)$. Here, the proceeding of GRR is also recognized by the color change from dark brown to dark blue. Typical TEM and SEM images of hAu nanoshells are shown in Fig. 1. Deposition of Au(s) on the outer surface of the Co nanoparticles is clear by showing a bright center surrounded with much darker shell, which confirms successful synthesis of hAu nanoshells (Fig. 1A) without significant size distribution (Fig. 1B). The mean outer diameter of hAu nanoshells was estimated as 57.9 ± 4.6 nm by sampling 50 nanoshells. For further modification, Ru precursor solution was added to the mixture solution containing hAu nanoshells, where the reaction time between Co nanoparticles and $HAuCl_4$ was reduced from 15 to 5 min and the color changed back to dark brown (see Section 2). After the reaction between hAu nanoshells and the Ru precursor, the hollow structure of hAu was maintained basically in hAu–Ru nanoshells (Fig. 2B). The averaged outer diameter of fifty hAu–Ru nanoshells was also measured to be 49.0 ± 4.7 nm, which is slightly smaller than that of hAu nanoshells owing to the reduced reaction time between Co nanoparticles and $HAuCl_4$.

The bulk atomic% ratio of Au:Ru was 90:10 based on the averaged EDS measurements at >20 locations. As-prepared hAu–Ru nanoshells were further characterized by XPS (not shown). The Au4f and Ru3d peaks were observed at 83.6 and 284.8 eV, respectively, with surface atomic% ratio of 29.9:70.1 indicating the effective surface modification of Ru on hAu nanoshells. It implies that Au frame structure is coated by Ru layer in hAu–Ru, where deposition of Ru on both outer and inner surface should be possible unlike in formation of hAu nanoshells. Extrusion and even distribution of Ru over Au surface are clearly shown in the HAADF-STEM EDS elemental mapping image of hAu–Ru nanoshells (Fig. 2D). Thus, we believe, $Ru^{3+}$ precursor should have undergone the second GRR with Au(s) according to EDS results [25]. Additionally, Raman spectrum in Fig. 3 for hAu–Ru nanoshells represents the three characteristic first order phonon modes for $RuO_2$ corresponding to $E_g$(520 $cm^{-1}$), $A_{1g}$(639 $cm^{-1}$), and $B_{2g}$(~700 $cm^{-1}$), respectively. In our structure, on the other hand, the band positions are slightly shifted from the highly single crystalline $RuO_2$ structure by ~10 $cm^{-1}$ partly due to the size effect or the bound nature with Au nanostructures. In the case of the latter phenomenon, the strong background intensity in our study suggests that the surface enhanced Raman scattering would be possible. Thus, it clearly confirms that the $RuO_2$ nanostructure exists on the Au hollow structure originated from the partial surface oxidation of the Ru metal nanostructures. In the XRD data, typical diffraction peaks corresponding to (1 1 1), (2 0 0), and (2 2 0) phases of the fcc crystal structure were observed for both hAu and hAu–Ru (Fig. 4). However, the *bulk* ratios of the relative intensities of (1 1 1):(2 0 0):(2 2 0) were 1.00:0.29:0.32 for hAu and 1.00:0.16:0.05 for hAu–Ru, exhibiting relatively significant reduction in the peaks of (2 0 0) and (2 2 0).

### 3.2. Voltammetric analysis of hAu and hAu–Ru nanoshells for nonenzymatic sensor

It is reported that AA is one of the critical interfering species in glucose detection especially for the gold based electrocatalysts [26,27]. Thus, to compare the different catalytic effect for the direct oxidation of glucose and AA, LSV curves were recorded at hAu and hAu–Ru modified electrode in 0.1 M PBS solution containing 5.0 mM glucose and 0.5 mM AA (Fig. 5). The normal physiological levels of glucose and AA are known as 3–8 and 0.06–0.08 mM, respectively [8,11]. Interestingly, oxidation of glucose preceded oxidation of AA at hAu/GC while the order became reverse at hAu–Ru/GC.

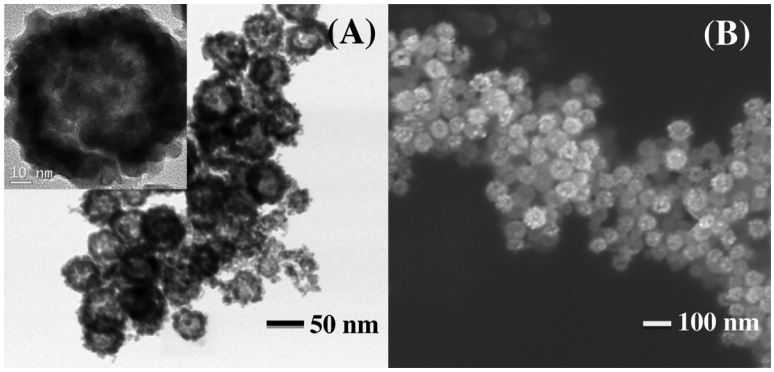


**Fig. 1.** Typical TEM (A) and SEM (B) images of hAu nanoshells.

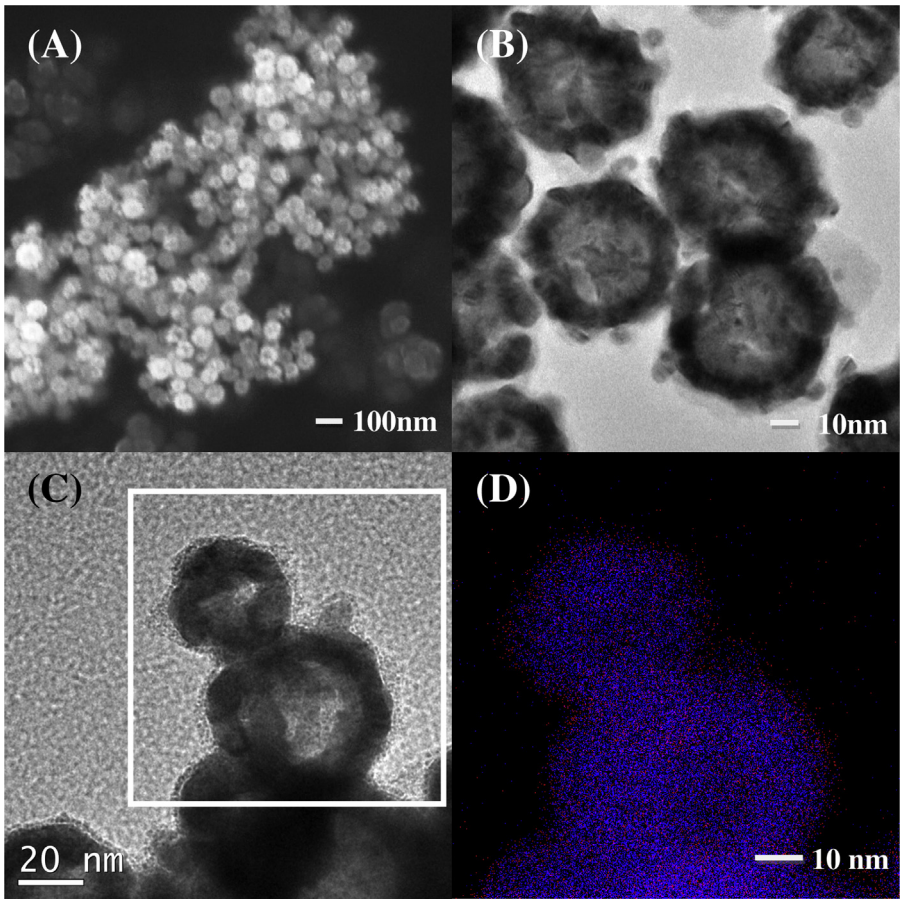


**Fig. 2.** SEM (A) and HR-TEM images (B, C) of hAu–Ru nanoshells. HAADF-STEM EDS elemental mapping image of hAu–Ru nanoshells (mapping area: white box in (C)) shown combine of Au (blue) and Ru (red) (D). (For interpretation of the references to color in this figure legend, the reader is referred to the web version of this article.)

In Fig. 5 anodic currents of glucose oxidation at both hAu/GC and hAu–Ru/GC decrease from 0.2 V to the more positive potential, which is well-known due to adsorption of glucose oxidation product on the gold surface [28,29]. In case of hAu–Ru/GC, the peak current at ca. 0.2 V is only 13% compared to that of hAu/GC case. Another anodic shoulder peak of glucose oxidation at ca. 0.0 V is known as oxidation at the nanostructured Au surface [27], which is virtually disappeared at hAu–Ru/GC unlike at hAu/GC probably due to difference of the surface property between hAu and hAu–Ru nanoshells. There is also recent report that the higher ratio of Ru in Au–Ru composite catalysts moves the oxidation potential of glucose to the more positive direction [30]. Based on the above discussion, it is reasonably concluded that major parts of surface of hAu–Ru nanoshells are covered by Ru and,

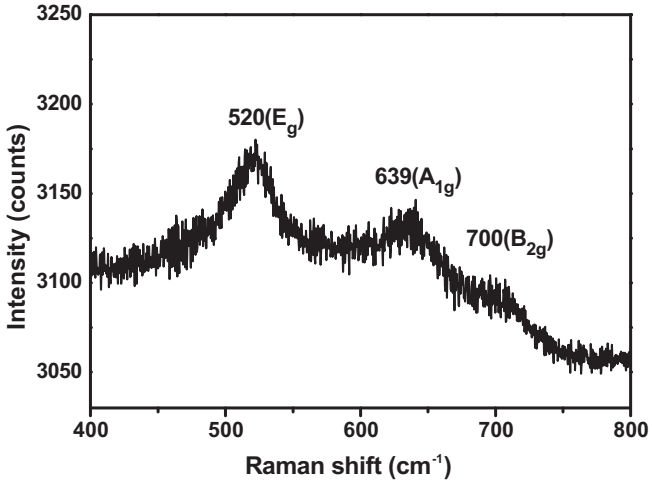


**Fig. 3.** Raman spectrum of hAu–Ru nanoshells measured at 632.8 nm with He–Ne laser.

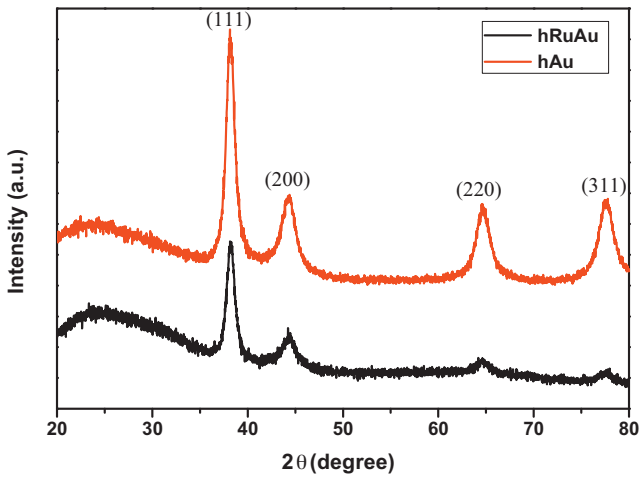


**Fig. 4.** XRD results for hAu–Ru and hAu.

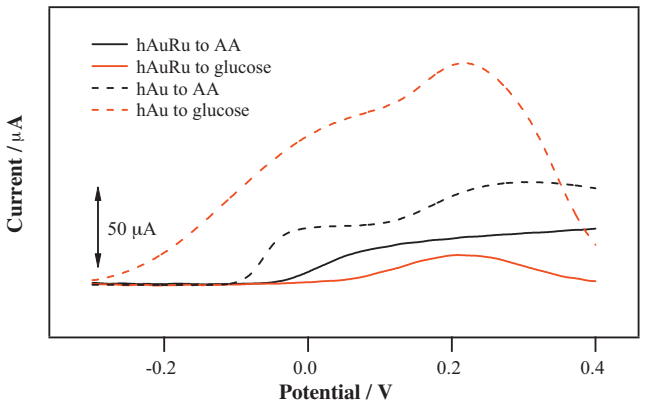


**Fig. 5.** Background-corrected LSVs using hAu–Ru/GC and hAu/GC in 0.1 M PBS containing 0.5 mM AA and 5 mM glucose. Potential scan rate was 5 mV $s^{-1}$ and rotating speed was 1600 rpm.

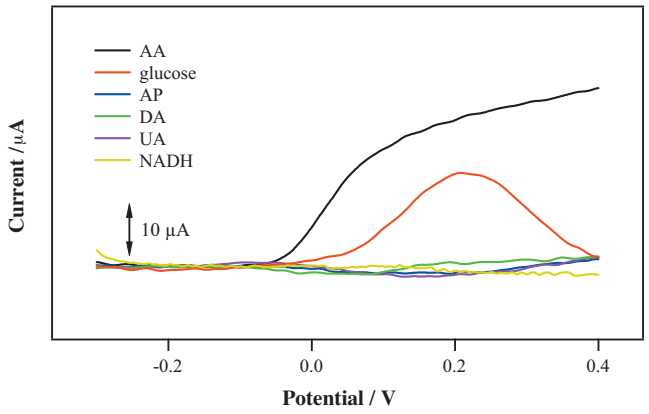


**Fig. 6.** Background-corrected LSVs using hAu–Ru/GC in 0.1 M PBS containing 0.5 mM AA, 5 mM glucose, 0.1 mM AP, 0.02 mM DA, 0.1 mM UA and 0.1 mM NADH. Potential scan rate was 5 mV $s^{-1}$ and rotating speed was 1600 rpm.

thereby, the characteristic oxidation of glucose on Au surface is well-suppressed at hAu–Ru/GC despite of 10% composition of Ru in bulk. On the other hand, oxidation current of AA at hAu–Ru/GC is relatively well-maintained compared to that at hAu/GC. Additionally, electroactivity of Au for the glucose oxidation was reported to depend on its crystal plane: Au (1 1 0) shows higher catalytic activity than the other crystal plane [28].

Based on the comparison of LSVs between hAu and hAu–Ru for glucose oxidation (Fig. S1 in Supplementary data), the pattern of glucose oxidation wave at hAu is observed to be similar to that on Au (1 1 0); on the other hand, the oxidation wave of glucose at hAu–Ru is similar to that on Au (1 1 1) reported [28]. This suggests that the significant portion of Au (1 1 0) surface plane, most active for glucose oxidation, is blocked by Ru during synthesis of hAu–Ru catalyst. It is also matched with the XRD data (Fig. 4) showing the suppressed peaks corresponding to (2 0 0) and (2 2 0) in hAu–Ru compared to hAu. Thus, it is proposed that the combination of Ru and Au decreases the catalyst activity for glucose oxidation especially for the potential region <0.2 V. To the contrast, hAu–Ru exhibits relatively less suppression in the catalytic activity for AA oxidation (at the potential region <0.2 V) compared to that for glucose oxidation. In fact, hAu–Ru induces a substantial shift of glucose oxidation potential to the positive direction with decreasing sensitivity and enables selective detection of AA against glucose at 0.05 V. As seen in Fig. S1, other interfering species are almost electrochemical-silent at 0.05 V. This implies that hAu–Ru/GC can be used as a potential amperometric sensor for AA without interference of glucose while hAu/GC shows a potential amperometric sensor characteristic for glucose free from interference of AA by control of electrode potential. In this report we are focusing on sensing of AA with hAu–Ru nanoshells and detailed electrochemical characteristic of hAu as nonenzymatic glucose sensing will be described elsewhere.

To show good performance of amperometric AA sensing in physiological condition, it is of importance to find the electrocatalytic material which enables the oxidation of AA at the lower potential than the oxidation of other interfering species [5]. As shown in Fig. 5, the oxidation of AA at hAu–Ru/GC starts at ca. −0.05 V which is lower potential than that at Pt electrode by 0.35 V [5].

To check the possibility of selective AA oxidation at hAu–Ru/GC, LSV experiments were performed against possible interferents such as glucose, AP, DA, UA, and NADH. The concentrations of glucose, AP, DA, UA, and NADH were 5, 0.1, 0.02, 0.1, and 0.1 mM, respectively, which were above the normal physiological levels. Fig. 6 presents the results of the above LSV experiments, where no considerable responses for the interferents were observed. As shown in Fig. 6, the only possible interfering species in amperometric AA detection is glucose among five interferents, which could be circumvented by control the detection potential as 0.05 V to maximize the response of AA oxidation and minimize that of glucose oxidation.

### 3.3. Amperometric response of hAu–Ru nanoshells to AA

Typical dynamic steady-state current response curves (*i*–*t* curves) to AA, glucose, AP, DA, UA and NADH were measured at hAu–Ru/GC in 0.1 M PBS and presented in Fig. 7A. Here, the AA concentration increased from 5 μM to 1.2 mM (Fig. 7A and C) by the successive additions of AA stock solution together with increasing the other interferent concentrations, respectively (see figure caption). While significant increasing oxidation current of AA was measured, glucose, AP, DA, UA and NADH were not detectable at 0.05 V as expected in LSV experiments. Fig. 7B and D show the corresponding calibration plots for amperometric AA detection at hAu–Ru/GC and the sensitivity of 30.1 μA $mM^{-1}$ was measured with $R = 0.9995$, which corresponds to 426 μA $mM^{-1}$ $cm^{-2}$ (normalized to the electrode disk area). Such a good linearity was maintained up to 2.0 mM (inset of Fig. 7B), which is a wide linear range considering that the physiological AA concentration for a healthy person is 0.06–0.08 mM. Response time (time required to achieve 95% current of its limiting current) and detection limit (S/N = 3) were measured from Fig. 7A as 1.6 s, and 2.2 μM, respectively. The current responses of hAu–Ru/GC to four different AA concentrations (50, 100, 150, and 200 μM) were measured via five separate runs and the calculated relative standard deviation (RSD) was <3.0%, indicating high reproducibility of this electrode (Fig. S2 and Table S1 in Supplementary data). In addition, we have also checked the reproducibility in terms of sensor by sensor. For the sensors prepared separately ($n = 5$), RSD of their sensitivity was <4.6 % (Table S2 in Supplementary data).

To investigate any interaction between interferents and AA or any obstructions in sensing AA, amperometric current response to AA was monitored while injecting various interferents as shown in Fig. 8. Indeed, no discernible changes in AA oxidation current were observed by the injection of glucose, AP, DA, UA or NADH except the injection of AA. The hAu–Ru nanoshells represented the same catalytic effect on AA oxidation regardless of presence or absence of interferents and can be considered as powerful enzyme-less sensor to estimate physiological concentration of AA with great selectivity and sensitivity.

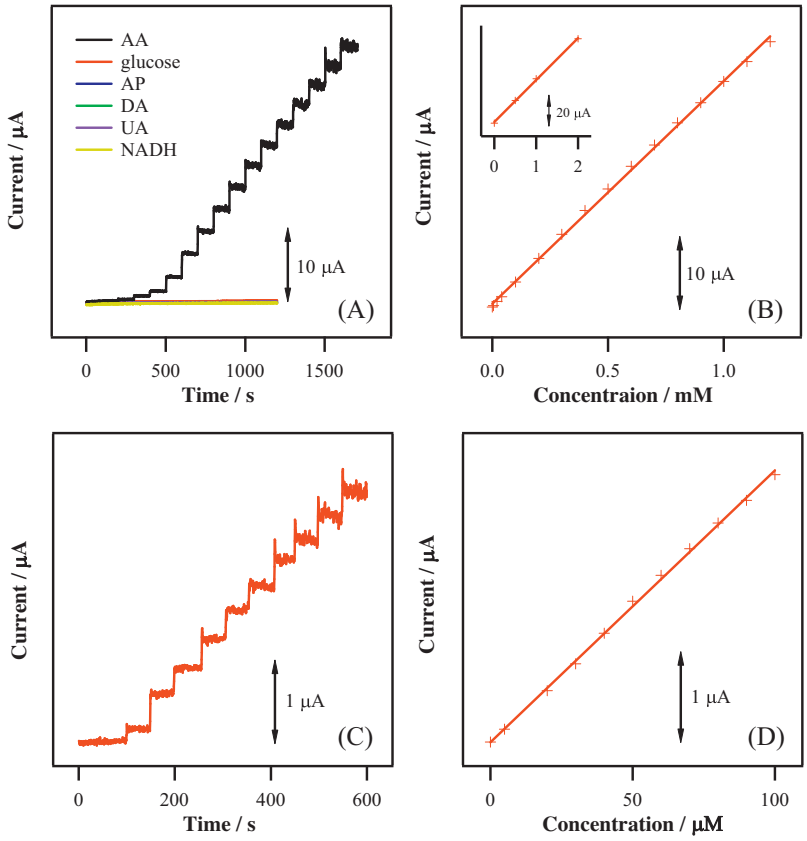


**Fig. 7.** Amperometric current responses to AA (0.05–1.2 mM), AP (0.05–0.5 mM), DA (0.001–0.01 mM), UA (0.05–0.5 mM), NADH (0.05–0.5 mM) and glucose (0.5–20 mM) (A); calibration curve to increase in AA concentration, Inset: wider range calibration (0.5–2 mM) (B). Responses to AA (0.005–0.1 mM) (C); calibration curve to increase in AA concentration (D) at the hAu–Ru/GC in 0.1 M PBS at potential of 0.05 V (vs. SCE).

Analytical performance of our AA sensor was compared with earlier reported nonenzymatic AA sensors (Table 1). AA sensor using hAu–Ru nanoshells showed good interference resistance under physiological condition. The operational stability of hAu–Ru/GC electrode for AA detection was tested. For this, the amperometric current was monitored at 0.05 V in 0.1 M PBS containing 0.3 mM AA as shown in Fig. 9. Over 95% of initial current was maintained for the prolonged period of >2500 s with some fluctuation due to stirring. Surprisingly, the high stability of hAu–Ru/GC electrode was observed even without any adhesion assisting chemicals (such as chitosan and Nafion), indicating the strong adsorption of hAu–Ru on GC. Finally, determination of AA contents in the real samples has been carried out using hAu–Ru on GC sensor to verify the praticability. For urine and vitamin C tablet samples, the analyses of AA amounts and recovery tests were performed by adding standard solution of AA. Table 2 summarizes the analysis and recovery tests of AA in these samples (see also Fig. S3).

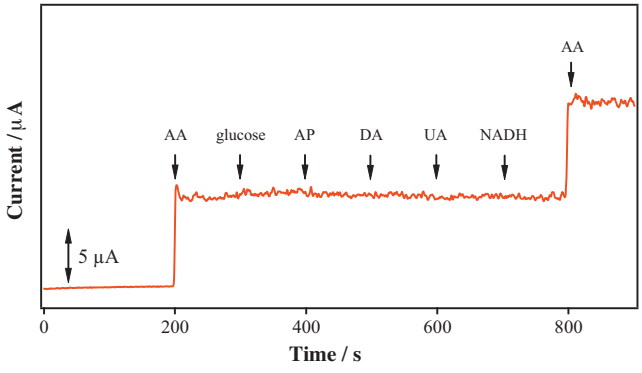


**Fig. 8.** Amperometric current responses at hAu–Ru/GC to the series of injection of 0.3 mM AA, 5 mM glucose, 0.1 mM AP, 100 nM DA, 0.1 mM UA, 0.1 mM NADH and 0.3 mM AA in 0.1 M PBS ($E_{appl}$ = 0.05 V (vs. SCE)).

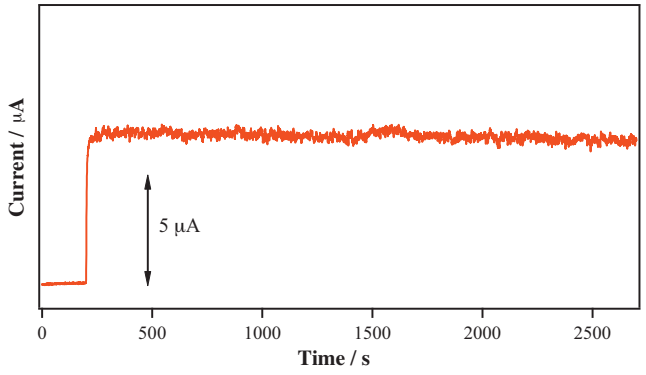


**Fig. 9.** Operational stability test of hAu–Ru/GC under continuous stirred solution of 0.3 mM AA in 0.1 M PBS at potential of 0.05 V (vs. SCE).

**Table 1**
Summary of the analytical performances of reported electrochemical AA detection systems.

| Ref. | Electrode | Sensitivity ($\mu A\,mM^{-1}$/ $\mu A\,mM^{-1}\,cm^{-2}$) | $E_{appl}$ vs. SCE (V) | Detection limit ($\mu M$) | Linear range (mM) | Solution | Interference test |
|---|---|---|---|---|---|---|---|
| This work | Hollow Au–Ru/GC | 30.1/426 | 0.05 | 2.2 | 0.005–2 | PBS (pH 7.4) | Glucose, AP, DA, UA, NADH |
| [7] | Poly(direct blue71)/GC | NR/NR | 0.14 | 1.0 | 0.001–2.0 | PBS (pH 7.0) | DA, UA |
| [9] | PPF/GNS | 18.5/260.56 | 0.33 | 120 | 0.4–6 | PBS (pH 7.0) | NR |
| [16] | Ultrathin Pd nanowire/GC | NR/166.5 | −0.04 | 0.2 | 0.025–0.9 | 0.1 M NaOH | Glucose, AP, UA, DA |
| [31] | MWNTs/Au NPs/HS$(CH_2)_6$Fc/GC | 26.3/NR | 0.35 | 0.1 | 0.0003–0.44 | PBS(pH 7.4) | UA |
| [32] | PAN–NSA/Pt | 1.62/NR | 0.30 | 12.93 | 5–60 | PBS (pH 7.0) | NR |
| [33] | $Cu^{2+}$A/ZCME/Pt | 34.54/NR | NR | 0.28 | 0.003–6.0 | oxalate buffer(pH 4.5) | UA, glucose, fructose, cysteine (interfered by NADH) |
| [34] | CuZEA/RGO/GC | NR/NR | −0.03 | 11 | 0.02–0.2 | PBS (pH 6.8) | DA |
| [35] | AC–RuOH–GC | 2.7/85.9 | −0.053 | NR | 0.047–0.1818 | PBS (pH 7.0) | DA, NAC |
| [36] | Screen-printing $RuO_2$ | 0.0838/2.79 | 0.058 | NR | 0–4 | PBS | UA, $H_2O_2$ |

NR = not reported.
PPF/GNS, pyrolysed photoresist film/graphene nano sheet; MWNTs/AuNPs, multiwalled carbon nanotubes–Au nanoparticles; Fc, ferrocene; GC, glassy carbon electrode; PAN–NSA, polyaniline–naphthalenesulfonic acid composite film; A/ZCME, zeolite type A modified electrode; ZEA/RGO, zeolite A/graphene oxide; AC–RuOH, acetaminophen on ruthenium oxide nanoparticles; NAC, *N*-acetyl-L-cysteine.

**Table 2**
Determination and recovery results of AA in real samples using hAu–Ru/GC sensor.

| Real sample | Injection amount from label (mM) | Found (mM) | Spiked AA (mM) | Recovery (%) |
|---|---|---|---|---|
| Urine (diluted 10 times) | – | 0.0427 ± 0.0049 | 0.1 | 97.8 |
| Vitamin C tablets | 0.2 | 0.205 ± 0.015 | 0.1 | 101.8 |

Results expressed as average ± standard deviation ($n = 5$).

## 4. Conclusions

We have successfully synthesized hollow Au–Ru nanoshells by modifying hAu nanoshells and described a novel nonenzymatic amperometric AA sensor candidate using as-prepared hAu–Ru nanoshells. We think that this work has three merits as following at least: (1) surface modification by Ru enabled AA sensing as a gold based electrocatalyst with high sensitivity for AA with 426 $\mu A\,mM^{-1}\,cm^{-2}$ (normalized to the disk area), linear dynamic range from <5.0 $\mu M$ to 2.0 mM ($R = 0.9995$), and fast response time (1.6 s) as well as low detection limit (2.2 $\mu M$); (2) almost perfect selectivity to AA against all possible physiological interferents, i.e., glucose, AP, DA, UA, and NADH, at pH 7.40; (3) such high sensitivity and selectivity were obtained without aid of enzyme, electron mediator, or other membranes. Overall, the hAu–Ru nanoshells appear to be a potential candidate material for a nonenzymatic AA sensor in physiological condition.

## Acknowledgments

This research was supported by Basic Science Program through the National Research Foundation of Korea (NRF) funded by the Ministry of Education, Science and Technology (No. 2013-020688 for CL and No. 2011-0015619 for YL).

## Appendix A. Supplementary data

Supplementary data associated with this article can be found, in the online version, at http://dx.doi.org/10.1016/j.aca.2014.02.017.

## References

[1] J. Zhang, H. Yang, G. Shen, P. Cheng, J. Zhang, S. Guo, Chemical Communications 46 (2010) 1112–1114.
[2] P. Begum, B. Fugetsu, Journal of Hazardous Materials 243 (2012) 212–222.
[3] H. Fetoui, M. Makni, E. Mouldi Garoui, N. Zeghal, Experimental and Toxicologic Pathology 62 (2010) 593–599.
[4] S.P. Arya, M. Mahajan, P. Jain, Analytica Chimica Acta 417 (2000) 1–14, and the references therein.
[5] A. Malinauskas, R. Garjonytė, R.I. Mažeikienė Jurevičiūtė, Talanta 64 (2004) 121–129, and the references therein.
[6] P.J. O'Connell, C. Gormally, M. Pravda, G.G. Guilbault, Analytica Chimica Acta 431 (2001) 239–247.
[7] S.A. Kumar, P. Lo, S. Chen, Biosensors and Bioelectronics 24 (2008) 518–523.
[8] N. Chauhan, J. Narang, C. Pundir, Analyst 136 (2011) 1938–1945.
[9] G.P. Keeley, A. O'Neill, N. McEvoy, N. Peltekis, J.N. Coleman, G.S. Duesberg, Journal of Materials Chemistry 20 (2010) 7864–7869.
[10] X. Luo, J. Xu, W. Zhao, H. Chen, Analytica Chimica Acta 512 (2004) 57–61.
[11] S. Park, T.D. Chung, H.C. Kim, Analytical Chemistry 75 (2003) 3046–3049.
[12] H. Boo, S. Park, B. Ku, Y. Kim, J.H. Park, H.C. Kim, T.D. Chung, Journal of the American Chemical Society 126 (2004) 4524–4525.
[13] S. Park, H. Boo, T.D. Chung, Analytica Chimica Acta 556 (2006) 46–57.
[14] J. Huang, Y. Liu, H. Hou, T. You, Biosensors and Bioelectronics 24 (2008) 632–637.
[15] S. Harish, J. Mathiyarasu, K. Phani, V. Yegnaraman, Journal of Applied Electrochemistry 38 (2008) 1583–1588.
[16] D. Wen, S. Guo, S. Dong, E. Wang, Biosensors and Bioelectronics 26 (2010) 1056–1061.
[17] G. Wu, Y. Wu, X. Liu, M. Rong, X. Chen, X. Chen, Analytica Chimica Acta 745 (2012) 33–37.
[18] W.A. El-Said, J. Lee, B. Oh, J. Choi, Electrochemistry Communications 12 (2010) 1756–1759.
[19] S. Zeng, K. Yong, I. Roy, X. Dinh, X. Yu, F. Luan, Plasmonics 6 (2011) 491–506.
[20] L. Zhang, X. Jiang, Journal of Electroanalytical Chemistry 583 (2005) 292–299.
[21] P. Kannan, S.A. John, Analytical Biochemistry 386 (2009) 65–72.
[22] D. Ragupathy, A.I. Gopalan, K. Lee, Sensors & Actuators, B: Chemical 143 (2010) 696–703.
[23] S.B. Aoun, Z. Dursun, T. Koga, G.S. Bang, T. Sotomura, I. Taniguchi, Journal of Electroanalytical Chemistry 567 (2004) 175–183.
[24] H. Liang, L. Wan, C. Bai, L. Jiang, The Journal of Physical Chemistry B 109 (2005) 7795–7800.
[25] J.H. Shim, A. Cha, Y. Lee, C. Lee, Electroanalysis 23 (2011) 2057–2062.
[26] B.S. Cho, C. Kang, Electroanalysis 19 (2007) 2315–2320.
[27] B. Seo, J. Kim, Electroanalysis 22 (2010) 939–945.
[28] M. Hsiao, R. Adžić, E. Yeager, Journal of the Electrochemical Society 143 (1996) 759–767.
[29] M. Pasta, F.L. Mantia, Y. Cui, Electrochimica Acta 55 (2010) 5561–5568.
[30] Q. Yi, W. Yu, F. Niu, Electroanalysis 22 (2010) 556–563.
[31] J. Qiu, R. Wang, R. Liang, M. Xiong, Electroanalysis 20 (2008) 1819–1824.

[32] L. Zhang, Electrochimica Acta 52 (2007) 6969–6975.
[33] T. Rohani, M.A. Taher, Talanta 78 (2009) 743–747.
[34] P. He, W. Wang, L. Du, F. Dong, Y. Deng, T. Zhang, Analytica Chimica Acta 739 (2012) 25–30.
[35] H.R. Zare, F. Chatraei, Sensors & Actuators, B: Chemical 160 (2011) 1450–1457.
[36] J. Wu, J. Suls, W. Sansen, Electrochemistry Communications 2 (2000) 90–93.